

Efficient Quantum Transport Simulation for Bulk Graphene Heterojunctions

Ming-Hao Liu (劉明豪) and Klaus Richter

Institut für Theoretische Physik, Universität Regensburg, D-93040 Regensburg, Germany

(Dated: March 11, 2017)

The quantum transport formalism based on tight-binding models is known to be powerful in dealing with a wide range of open physical systems subject to external driving forces but is, at the same time, limited by the memory requirement increasing with the number of atomic sites in the scattering region. Here we demonstrate how to achieve an accurate simulation of quantum transport feasible for experimentally sized bulk graphene heterojunctions at a strongly reduced computational cost. Without free tuning parameters, we show excellent agreement with a recent experiment on Klein backscattering [A. F. Young and P. Kim, *Nat. Phys.* **5**, 222 (2009)].

PACS numbers: 72.80.Vp, 73.23.Ad, 73.40.Gk, 72.10.Bg

Electronic transport is one of the important fields among the increasing amount of fundamental studies [1, 2] of graphene, a one-atom-thick carbon honeycomb lattice [3]. Due to the gapless and chiral nature of its electronic structure, graphene exhibits energy dispersions linear in momentum, the transport carriers behave like massless Dirac fermions, and the properties based on Schrödinger wave mechanics in semiconductor physics have to be retreated by Dirac-type physics in graphene. Tunneling across *pn* and *pnp* junctions is perhaps the most popular example that tells how different the charge carriers behave, as compared to semiconductor heterostructures. By solving the Dirac equation for transmission through a potential barrier, Katsnelson *et al.* showed the absence of backscattering at normal incidence in monolayer graphene [4]. This mimicks the Klein paradox in quantum electrodynamics [5] and was later on referred to as Klein tunneling [6, 7], which attracted both experimental [8–14] and further theoretical [15–23] investigations.

The Dirac theory, an effective approach valid only for low-energy excitations, generally serves as a starting point for theoretical studies of transport in graphene and can often provide analytical results to capture basic physical insights for certain problems with simplified system geometries. For further considerations, to account for complicated geometries and more realistic factors, one has to resort to more advanced theoretical models. The tight-binding model (TBM), a commonly used semi-empirical approach for electronic structure calculations in solid state physics [24], allows for consideration of more complete band information of graphene at low computational cost. The combination of the TBM with nonequilibrium Green's function approaches forms the modern quantum transport formalism [25] that is able to deal with a wide range of conductors composed of a scattering region and external leads with or without bias. The description of the graphene scattering region of interest, however, requires a TBM Hamiltonian matrix,

$$\mathcal{H}_{\text{gnr}}(V, t, t') = \sum_{n=1}^N V_n c_n^\dagger c_n - t \sum_{\langle m, n \rangle} c_n^\dagger c_m - t' \sum_{\langle\langle m, n \rangle\rangle} c_n^\dagger c_m, \quad (1)$$

whose matrix size depends on the involved number of atomic sites N and imposes therefore a computational limit when ad-

ressing realistic experimental system sizes. This is partly the reason why many quantum transport studies address graphene “nanoribbons” rather than large-area graphene.

Typical sizes of graphene flakes for experimental transport investigations amount to a few microns by a few microns, but even a $1 \mu\text{m} \times 1 \mu\text{m}$ graphene flake contains roughly 10^7

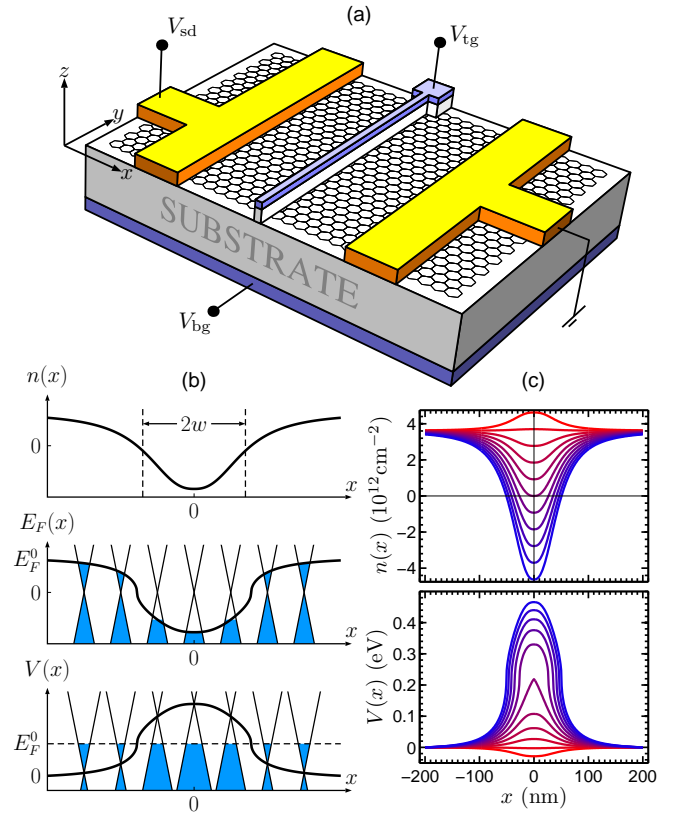


FIG. 1. (Color online) (a) Schematic of double-gated graphene. (b) Carrier density profile $n(x)$ (top) and its corresponding local Fermi level $E_F(x)$ (middle). The extracted potential profile $V(x)$ (bottom) is given by the difference of the global Fermi level E_F^0 and $E_F(x)$; see text. (c) Reproduced densities $n(x)$ (top) provided in the supplementary material of Ref. 13 with $V_{bg} = 50 \text{ V}$ and $V_{tg} = -8.9, -7.9, \dots, 0.1, 1.1 \text{ V}$ (from bottom to top curves), and the extracted corresponding $V(x)$ (bottom).

atoms, leading to a spinless single-orbital TBM Hamiltonian matrix of more than 10^{14} elements that requires an exceeding memory and hence an unreasonable computation burden. TBM-based quantum transport for bulk materials therefore requires further improvements to overcome the issue of the limited scattering region size. In this paper, we demonstrate how an accurate TBM-based transport calculation for bulk graphene heterojunctions can be performed without free parameters, circumventing the problem of large system scales. Specifically, we choose the recent Klein backscattering experiment [13] for transport through double-gated graphene [as depicted in Fig. 1(a)] to compare with and to demonstrate our approach. To achieve such a TBM bulk transport simulation, two crucial concepts are required, which are described in the following.

Extraction of a realistic potential profile.— A theoretical study of transport in graphene, whether based on Dirac theory or TBM formalism, requires the potential $V(x)$ as an input, which actually means the local energy offset of the Dirac point and is often regarded directly as the electric potential. In fact, the application of a gate voltage V_g does not directly raise the Dirac cone by $-eV_g$ ($-e$ being the electron charge) but enhances or depletes the carrier density, hence raising or lowering the local Fermi level. For double-gated graphene [Fig. 1(a)], the combination of a top-gate voltage V_{tg} and a back-gate voltage V_{bg} results in a carrier density profile $n(x)$ such as that shown in the upper panel in Fig. 1(b). Its energy dependence, $n(E) = \text{sgn}(E) E^2 / [\pi(\hbar v_F)^2]$, is obtained by integrating the density of states over energy. Defining the local Fermi level as

$$E_F(x) = \text{sgn}[n(x)] \hbar v_F \sqrt{\pi |n(x)|}, \quad (2)$$

one obtains the spatially varying height of the filled states, as depicted in the middle panel in Fig. 1(b). In a transport calculation, the global Fermi level E_F^0 is a fixed quantity. Hence to account for the profiles of $E_F(x)$ and $n(x)$, one shifts the local band offset by applying a local potential

$$V(x) = E_F^0 - E_F(x), \quad (3)$$

as depicted in the lower panel of Fig. 1(b). This completes the extraction of the potential profile from the carrier density profile. A realistic carrier density profile depends on the experimental geometry and dielectric material of the gate fabrication. In the experiment of Ref. 13, $n(x)$ was obtained from an electrostatic simulation and empirically described by

$$n(x) = \left(\frac{12.8 V_{tg}}{1 + |x/w|^{2.5}} + V_{bg} \right) C_{bg}, \quad (4)$$

where 12.8 accounts for the effectiveness of the top-gate relative to the back-gate, $C_{bg} \approx 7.23 \times 10^{10} \text{ cm}^{-2}/\text{V}$ is the capacitance for graphene on a 290 nm-thick SiO_2 substrate, and the effective half width of the top-gate is $w = 46 \text{ nm}$ [13]. Figure 1(c) shows various carrier density profiles described by Eq. (4), subject to $V_{bg} = 50 \text{ V}$ and various V_{tg} , and the extracted potential profiles, Eqs. (2,3).

Bulk graphene scattering region.— In band theory, the electronic structure of a crystal lattice can be solved by applying the Bloch theorem, which allows us to reduce the problem with infinitely repeated unit cells to only one due to translation invariance along each space dimension. For transport calculations, however, the scattering region of interest is composed of a certain finite-size area and is generally not translationally invariant. For a large flake of double-gated graphene, such as that sketched in Fig. 1(a), the transverse dimension (along y) is typically a few microns in width so that the edges are of minor importance, and we can then assume translational invariance in y -direction. Consider bulk graphene oriented with zigzag carbon chains along the x direction. Up to nearest neighbor hopping, the minimal unit cell can be chosen as one hexagon row, i.e., a graphene nanoribbon with zigzag chain number $N_z = 2$ with transverse periodicity $W = 3a$, $a \approx 1.42 \text{ \AA}$ being the bond length. The wave function at the bottom site $\langle x, y_B | \varphi \rangle$ of the unit cell is related to that at the top site $\langle x, y_T | \varphi \rangle$ through the Bloch theorem as [26] $\langle x, y_T + a | \varphi \rangle = e^{ik_y W} \langle x, y_B | \varphi \rangle$, implying $|x, y_T\rangle \langle x, y_T + a| = e^{ik_y W} |x, y_T\rangle \langle x, y_B|$, where k_y is the Bloch momentum defined within $k_y W \in [-\pi, \pi]$. This means that a kinetic hopping across the upper boundary of the unit cell $|x, y_T\rangle \langle x, y_T + a|$ can be equivalently expressed as a periodic hopping $|x, y_T\rangle \langle x, y_B|$ modulated by the phase $e^{ik_y W}$ arising from the Bloch theorem. Similarly, one can obtain for the lower boundary $|x, y_B\rangle \langle x, y_B - a| = e^{-ik_y W} |x, y_B\rangle \langle x, y_T|$. Incorporating these periodic hopping terms, the TBM Hamiltonian for a bulk graphene scattering region can therefore be written as

$$\mathcal{H}_{\text{bulk}}(V, t; k_y) = \mathcal{H}_{\text{gnr}}(V, t, 0) + \left(-t e^{ik_y W} \sum_m c_{T_m}^\dagger c_{B_m} + \text{H.c.} \right), \quad (5)$$

where $c_{T_m}^\dagger$ (c_{B_m}) creates (annihilates) a charge carrier at the top (bottom) edge site of the m th hexagon along x , and $\mathcal{H}_{\text{gnr}}(V, t, 0)$, given in Eq. (1), describes a $N_z = 2$ graphene nanoribbon. Note that the above description for a bulk scattering region is neither restricted to nearest neighbor hopping ($t' = 0$), nor to the material graphene.

The quantum transport simulation in the present work will be restricted to the linear response regime at zero temperature. Thus the Landauer conductance

$$g(E_F^0) = \frac{e^2/h}{2k_F} \int_{-k_F}^{k_F} T(E_F^0; k_y) dk_y \quad (6)$$

will be the main object and is obtained by integrating the transmission function

$$T(E; k_y) = \text{Tr}(\Gamma_L G_R \Gamma_R G_L^\dagger), \quad (7)$$

which is equivalent to the Fisher-Lee relation [27]. The Fermi wave vector in Eq. (6) will be approximated from the low-energy linear dispersion by $k_F = E_F^0 / (\hbar v_F) = E_F^0 / (3ta/2)$.

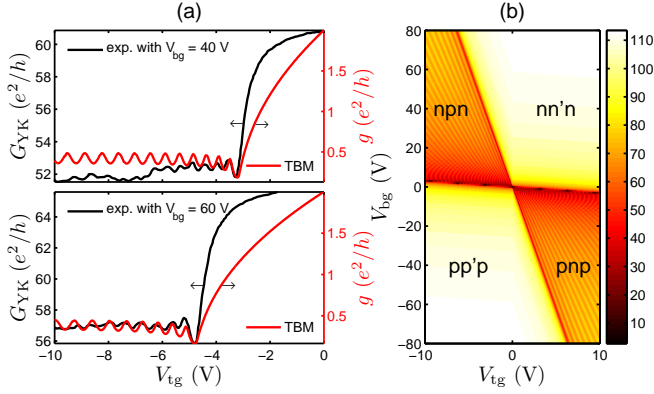


FIG. 2. (Color online) (a) Comparison of the top-gate voltage dependence of the measured conductance G_{YK} [28] and the computed single-mode conductance g at $V_{bg} = 40$ V and $V_{bg} = 60$ V. (b) Conductance map of $G(V_{tg}, V_{bg}) = [(M \cdot g)^{-1} + R_c]^{-1}$, where the number of modes is given by $M(E) = 2L_y |E| / (\pi \hbar v_F)$, assuming an effective width $L_y = 2 \mu\text{m}$ and contact resistance $R_c = 0.2 \text{ k}\Omega$.

Note that the spin degeneracy is neglected here, while the valley degeneracy is inherently incorporated in $\mathcal{H}_{\text{bulk}}$.

The retarded Green's function G_R of the scattering region at energy E in Eq. (7) is obtained from

$$G_R(E; k_y) = \frac{1}{E - [\mathcal{H}_{\text{bulk}}(V, t; k_y) + \Sigma_L + \Sigma_R]}, \quad (8)$$

where $\mathcal{H}_{\text{bulk}}(V, t; k_y)$ has been given in Eq. (5) and Σ_L (Σ_R) is the self-energy due to the left (right) lead composed of a semi-infinite repetition of unit cells. Adopting a Schur-decomposition-based algorithm for the singular hopping matrix type [26], the periodic hoppings as used in $\mathcal{H}_{\text{bulk}}$ can also be included in Σ_L and Σ_R , enabling us to study pure bulk-to-bulk transmission. The spectral matrix functions Γ_l with $l = L, R$ in Eq. (7) are given by $\Gamma_l = i(\Sigma_l - \Sigma_l^\dagger)$.

Now we revisit the experiment of Ref. 13 by considering the extracted realistic potential $V(x)$ and applying the bulk TBM transport formalism introduced above. As already shown in Fig. 1(c), the potential profile saturates at roughly ± 200 nm, so we consider a scattering region described by $\mathcal{H}_{\text{bulk}}(V(x), t; k_y)$ with length $L_x = 400$ nm. The transport is solely supported by the states at the global Fermi level, which is set to $E_F^0 = E_F$ ($x = \pm 200$ nm). We first investigate the top-gate voltage dependence of the single-mode conductance g . In Fig. 2(a), we directly compare the oscillating features of our computed g with the experimental data G_{YK} [28], choosing the measured $G_{YK}(V_{tg}, V_{bg} = 40$ V) and $G_{YK}(V_{tg}, V_{bg} = 60$ V) curves as explicit examples. In both cases, the general features of the measured oscillating conductance are well captured by our TBM calculation. The Dirac point position of the locally-gated region corresponds to the conductance dip. To the left of this minimum the transport is in the *npn* regime exhibiting Fabry-Pérot-type oscillations due to interference of backscattered waves between the *np* and *pn* interfaces. To the right of the dip, the transport enters the

nn'n regime, where graphene becomes much more transparent than for *npn*, resulting in the suppression of the interference and the rise of the conductance. This conductance asymmetry [8, 12, 18, 29] is the first indirect feature of Klein tunneling, which results in the decay of the transmission with the incident angle in the *np* regime [15] and hence a lower integrated conductance, although the tunneling at normal incidence is perfect.

The single-mode spin-degenerate conductance g from Eq. (6) has a maximum of $2e^2/h$ and does not reflect the effect of the back-gate voltage that tunes the global Fermi level E_F^0 , as well as the number of modes M participating in transport. For bulk graphene at low energy, M can be approximated by $2k_F/\Delta k_y$ with $\Delta k_y = 2\pi/L_y$, where L_y is the width of the graphene flake. This gives $M(E) = 2L_y |E| / (\pi \hbar v_F)$. While the calculation considers the bulk transport across the locally gated region in graphene, the contact resistance R_c between the electrodes and graphene is not included. To compare with the full map of the measured $G_{YK}(V_{tg}, V_{bg})$, we adopt a simple model to account for multiple modes and contact resistance: $G(E_F^0) = \{[M(E_F^0)g(E_F^0)]^{-1} + R_c\}^{-1}$. Assuming an effective width $L_y = 2 \mu\text{m}$ and a low contact resistance $R_c = 0.2 \text{ k}\Omega$, we display the calculated top- and back-gate dependencies of $G(E_F^0)$ in Fig. 2(b), which qualitatively agrees with Ref. 13. Note that the quadrants of $G(V_{tg}, V_{bg})$ are given by the dependence of the potential profile on V_{tg} and V_{bg} , and do not significantly change with different L_y and R_c .

Finally, we come to a closer analysis of the low-field magnetotransport. For an *incoherent* graphene *pnp* junction a perpendicular magnetic field leads to the increase of the magnetoresistance due to the bending of the electron trajectories [15]. When the top-gate is narrow enough, such as that in Ref. 13 with a width about 20 nm, a *coherent* graphene *pnp* junction can be formed. Shytov *et al.* [17] proposed a clever way to experimentally test the existence of Klein tunneling, making use of the sign change of the Klein backscattering phase at a weak magnetic field, which in turn results in a half-period shift of the Fabry-Pérot oscillations. Based on this semiclassical treatment the low-field magnetotransport experiment of Ref. 13 was regarded as giving evidence of Klein tunneling. In the following we show that our tuning-parameter-free TBM calculation confirms the semiclassical picture and again agrees well with the measurement.

The orbital contribution of the external magnetic field B_z perpendicular to the graphene plane is incorporated in the TBM calculation through the Peierls substitution [30], while the Zeeman term is neglected since the Zeeman splitting is rather small compared to E_F^0 [2]. To maintain the transverse (y) translation invariance throughout the whole system while keeping also the longitudinal (x) translation invariance in the leads, we consider the Landau gauge of $\mathbf{A} = (0, xB_z, 0)$ only in the scattering region. Inside the left and right leads, however, constant gauge field strengths $A_y^L = x_L B_z$ and $A_y^R = x_R B_z$ must be considered, respectively, where x_L and x_R are the position coordinates of the left-most and right-most atomic site of the scattering region, in order to avoid a discon-

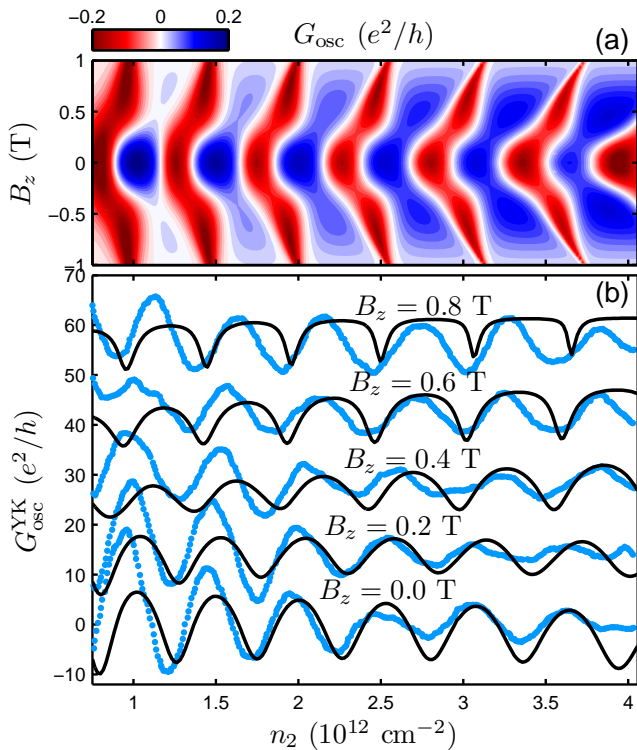


FIG. 3. (Color online) (a) Oscillating part of the computed conductance $G_{\text{osc}}(n_2, B_z)$ (see text for definition) as a function of carrier density of the locally gated region $n_2 \equiv n(x=0)$ and the external magnetic field B_z . (b) Comparison of computed G_{osc} curves (solid black curves) at various magnetic field strengths with the experimental data of Ref. 13 [blue (gray) dots].

tinuity of the vector potential.

Since the expected phase shift stems from Klein backscattering between the two interfaces inside the locally gated region, the potential tail does not play a crucial role and we reduce the scattering region length to $L_x = 150$ nm. Following the definition of the oscillating part of the conductance given in Ref. 13, we process our data of the single-mode conductance g by first computing the odd part of the conductance, $G_{\text{odd}}(n_2, B_z) = g(n_2, B_z) - g(-n_2, B_z)$, and then subtracting its mean value to obtain $G_{\text{osc}}(n_2, B_z) = G_{\text{odd}}(n_2, B_z) - \overline{G_{\text{odd}}(n_2, B_z)}$. Here $n_2 = n(x=0)$ [see Eq. (4)] is the carrier density of the locally-gated region. The obtained oscillation fringes of $G_{\text{osc}}(n_2, B_z)$ are shown in Fig. 3(a), which is again qualitatively consistent with Ref. 13. The sudden phase shift, which indicates the presence of perfect transmission and corresponds to the half-period shift predicted by Shytov *et al.* [17], occurs at magnetic field strengths between 0.2 T and 0.4 T and is in excellent agreement with Ref. 13. In Fig. 3(b), the computed G_{osc} is compared with the experimental data $G_{\text{osc}}^{\text{YK}}(n_2, B_z)$ [28] at various magnetic field strengths (both with offset for clarity).

In conclusion, we have demonstrated the applicability of TBM-based quantum transport simulations for transport in bulk graphene heterojunctions. Applying the Bloch theorem

along the transverse dimension, the computational effort for TBM transport through a bulk scattering region is significantly reduced. Together with the realistic potential profile extracted from the carrier density profile of a graphene *pn*p junction, this method provides a confirmation of the experiment of Ref. 13, without using free tuning parameters and at low computational cost. The quantum transport approach presented here for studying bulk properties is suitable not only for graphene but also for other materials where the TBM works well.

We appreciate valuable discussions with A. Cresti and V. Krueckl. Financial support from Alexander von Humboldt Foundation (M.H.L.) and Deutsche Forschungsgemeinschaft within GRK1570 (K.R.) is gratefully acknowledged.

-
- [1] A. H. Castro Neto, F. Guinea, N. M. R. Peres, K. S. Novoselov, and A. K. Geim, *Rev. Mod. Phys.* **81**, 109 (2009).
 - [2] S. Das Sarma, S. Adam, E. H. Hwang, and E. Rossi, *Rev. Mod. Phys.* **83**, 407 (2011).
 - [3] K. S. Novoselov, A. K. Geim, S. V. Morozov, D. Jiang, Y. Zhang, S. V. Dubonos, I. V. Grigorieva, and A. A. Firsov, *Science* **306**, 666 (2004).
 - [4] M. I. Katsnelson, K. S. Novoselov, and A. K. Geim, *Nat. Phys.* **2**, 620 (2006).
 - [5] O. Klein, *Zeitschrift für Physik* **53**, 157 (1929).
 - [6] C. W. J. Beenakker, *Rev. Mod. Phys.* **80**, 1337 (2008).
 - [7] P. Allain and J. Fuchs, *Eur. Phys. J. B* **83**, 301 (2011).
 - [8] B. Huard, J. A. Sulpizio, N. Stander, K. Todd, B. Yang, and D. Goldhaber-Gordon, *Phys. Rev. Lett.* **98**, 236803 (2007).
 - [9] J. R. Williams, L. DiCarlo, and C. M. Marcus, *Science* **317**, 638 (2007).
 - [10] B. Özyilmaz, P. Jarillo-Herrero, D. Efetov, D. A. Abanin, L. S. Levitov, and P. Kim, *Phys. Rev. Lett.* **99**, 166804 (2007).
 - [11] G. Liu, J. J. Velasco, W. Bao, and C. N. Lau, **92**, 203103 (2008).
 - [12] N. Stander, B. Huard, and D. Goldhaber-Gordon, *Phys. Rev. Lett.* **102**, 026807 (2009).
 - [13] A. F. Young and P. Kim, *Nat. Phys.* **5**, 222 (2009).
 - [14] S.-G. Nam, D.-K. Ki, J. W. Park, Y. Kim, J. S. Kim, and H.-J. Lee, *Nanotechnology* **22**, 415203 (2011).
 - [15] V. V. Cheianov and V. I. Fal'ko, *Phys. Rev. B* **74**, 041403 (2006).
 - [16] L. M. Zhang and M. M. Fogler, *Phys. Rev. Lett.* **100**, 116804 (2008).
 - [17] A. V. Shytov, M. S. Rudner, and L. S. Levitov, *Phys. Rev. Lett.* **101**, 156804 (2008).
 - [18] T. Low, S. Hong, J. Appenzeller, S. Datta, and M. S. Lundstrom, *IEEE Trans. Electron Devices* **56**, 1292 (2009).
 - [19] A. Yamakage, K. I. Imura, J. Cayssol, and Y. Kuramoto, *EPL* **87** (2009).
 - [20] T. Low and J. Appenzeller, *Phys. Rev. B* **80**, 155406 (2009).
 - [21] E. Rossi, J. H. Bardarson, P. W. Brouwer, and S. Das Sarma, *Phys. Rev. B* **81**, 121408 (2010).
 - [22] M. Ramezani Masir, P. Vasilopoulos, and F. M. Peeters, *Phys. Rev. B* **82**, 115417 (2010).
 - [23] M.-H. Liu, J. Bundesmann, and K. Richter, *Phys. Rev. B* **85**, 085406 (2012).
 - [24] G. Grosso and G. P. Parravicini, *Solid State Physics* (Academic Press, New York, 2000).
 - [25] S. Datta, *Electronic Transport in Mesoscopic Systems* (Cam-

bridge University Press, Cambridge, 1995).

- [26] M. Wimmer, *Quantum transport in nanostructures: From computational concepts to spintronics in graphene and magnetic tunnel junctions*, Ph.D. thesis, Universität Regensburg (2008).
- [27] D. S. Fisher and P. A. Lee, Phys. Rev. B **23**, 6851 (1981).
- [28] The experimental data compared in this work were extracted from the electronic file of Ref. 13, instead of the original data.
- [29] J. Cayssol, B. Huard, and D. Goldhaber-Gordon, Phys. Rev. B **79**, 075428 (2009).
- [30] R. Peierls, Z. f. Phys. A **80**, 763 (1933).